Electronic Supplementary Information

An Efficiently Tuned d-Orbital Occupation of IrO_2 by Doping Cu for Enhancing Oxygen Evolution Reaction Activity

Wei Sun[a], Ya Song[b], Xue-Qing Gong[b,†], Li-mei Cao[a], Ji Yang[a,†]

[a]State Environmental Protection Key Laboratory of Environmental Risk Assessment and Control on Chemical Processes, School of Resources and Environmental Engineering, East China University of Science and Technology, 130 Meilong Road Shanghai 200237, P.R. China, [b]Key Laboratory for Advanced Materials, Center for Computational Chemistry and Research Institute of Industrial Catalysis, East China University of Science and Technology, 130 Meilong Road, Shanghai 200237, P.R. China

[†]To whom correspondence should be addressed.

Corresponding authors' E-mail: yangji@ecust.edu.cn; xgong@ecust.edu.cn

Experimental Section

Materials synthesis: The IrO_2 catalysts doped with Cu, IrO_2 and CuO materials were synthesized using hydrothermal methods and annealed at 600°C with a 6-h dwell time to produce good crystallinity. For preparing the composition $Cu_xIr_{1-x}O_\delta$ (x=0-1, δ=2-1), $Cu(NO_3)_2$ at 113.4 mmol/L and $IrCl_3 \cdot 3H_2O$ at 56.7 mmol/L in variable stoichiometric amounts were mixed into a 40-mL Teflon-lined pressure vessel with 10 mL deionized water and 5 mL 0.5 M aqueous NaOH. The mixture was loaded into an oven to heat the solution to 250°C for 720 min; then, the vessels were cooled naturally at room temperature. The precipitates were suction filtered and washed with deionized water twice to remove other ions. The remaining solid on the filter was dried to dehydration in an oven at 80 °C for 1 h. The dried solid was transferred to a crucible and annealed at 600 °C for 6 h to produce excellent crystallinity due to the hydrothermal precipitates that were identified as amorphous using the powder XRD data.

Electrode Preparation and Electrochemical Measurements. In this study, the electrodes used for the electrochemical measurements were of the so-called dimensionally stable anode (DSA) type, which were prepared as follows. 6 mg of fresh catalyst powders of $Cu_xIr_{1-x}O_\delta$ were dispersed in 1.5 mL of 2:1 v/v isopropanol / water and then ultrasonicated for approximately 1 h to form a homogeneous ink. Next, 7.5 μL of ink deposited on 0.5 cm × 1.5 cm Ti plate, which was etched for 2 h by 10% (wt %) oxalic acid under near boiling conditions and then washed with deionized water. The process was repeated 5 times to obtain a loading weight of approximately 0.2 mg/cm^2 and was then stabilized by annealing for 20 minutes at 400 °C on each cycle. All electrochemical measurements were conducted using a three–electrode cell. The working electrode used was 0.5 cm × 0.5 cm (electrode reactive area = 0.25 cm^2) of the prepared DSA, and the remaining was insulated, except for a small part for connecting the wire. Here, a saturated calomel reference electrode (SCE) and a polished and cleaned Pt foil with a 1.5 cm × 1 cm reaction area were used for the counter electrode. The electrode potential from the SCE scale was converted to the reversible hydrogen electrode (RHE) scale by calibrating with: E (RHE) = E (SCE) + $E_{j=0}$. The over-potential values (η) corrected with the iR were obtained using the following equation: $\eta = E_{Applied}$ (RHE) – iR-1.229, where i is the current, and R is the uncompensated Ohmic electrolyte resistance and was measured via AC impendence at the open circuit potential with 10 mV amplitude in three different pH solutions. The working electrodes were cycled a least 5 times until the curves were observed to overlap; then, the data of the CV's and polarization curves were recorded at the specified scan rate. The Tafel plots were conducted by the stair-case voltammetry method at the different potential range (vs. RHE), with 10 mV steps every 100 s (scan rate 0.1 mV/s) and current values were read at the end of each step. The electrolytes included 0.1 M $HClO_4$ (pH~1), 38 mL 0.2 M NaH_2PO_4 and 62 mL 0.2 M Na_2HPO_4 (pH~7), 0.1 M KOH (pH~13) and all of the chemicals were of analytical grade. In addition, deionized water was employed as the solvent; all chemicals used were of analytical grade, and the solvent used was deionized water.

Characterization. Except the OER activity, all the characterizations of the catalysts were performed for samples annealed at 600°C, before anchored on the Ti plate. The crystal structure of the catalysts were investigated using powder X-Ray diffraction (XRD) using a D/max2550 V apparatus with a Cu-Kα radiation source (λ=1.5406 Å), and the data were recorded over a range of 10 to 80° at a step size of 0.02°. The morphologies of the catalysts were observed using a field-emission scanning electron microscope (FESEM) equipped with a Nova NanoS and the Energy dispersive X-ray (EDX) spectrometer to confirm the composition using a TEAMApollo system. A JEM-2100 transmission electron microscope was used to obtain the TEM and HRTEM images. The surface properties of the catalysts were determined via X-ray photoelectron spectroscopy (XPS) using an ESCALAB 250Xi instrument with an Al-Kα radiation source at an energy step size of 0.05 eV for high resolution XPS spectrum. The samples were sputter coated with carbon, and the spectra were calibrated with respect to C-*1s* at a binding energy

of 284.6 eV. The X-ray absorption data (XAS) at the Ir L_{III} edge and the Cu K edge of the samples, which were mixed with LiF to reach 50 mg, were recorded at room temperature in transmission mode using ion chambers using the BL14W1 beam line of the Shanghai Synchrotron Radiation Facility (SSRF), China. The station was operated with a Si (111) double crystal monochromator. During measurements, the synchrotron was operated at an energy of 3.5 GeV and a current between 150-210 mA.

RHE calibration: The SCE was calibrated with respect to the RHE in all three types of pH solution using a high purity hydrogen saturated electrolyte with a Pt foil as the working electrode[1]. CVs were run at a scan rate of 1 mV/s, and the average of the two potentials at which the current crossed zero was recorded to as the thermodynamic potential for the hydrogen electrode reaction.

Computational Details

All first-principle calculations were performed using the density functional theory (DFT) methodology implemented in the Vienna Ab-initio Simulation Package (VASP). The spin-polarized projector augmented wave (PAW) method[2, 3] and the Perdew-Burke-Ernzerhof (PBE)[4, 5] electron exchange-correlation functional of the generalized gradient approximation (GGA) were used in these calculations. The energy cutoff for the wave function expanding in the plane-wave basis was set to 400 eV. The energetic convergence threshold for the self-consistent field (SCF) was 1×10^{-4} eV/atom, and atomic relaxation was performed until all components of the residual forces were less than 0.05 eV/Å. For the surface models, the vacuum slab height between the slabs was ~20 Å to eliminate the interaction between neighboring slabs. The valence electronic configurations considered in this study were Ir (5*d*, 6*s*), O (2*p*, 2*s*), Cu (3*d*, 4*p*) and H (1*s*).

A $\sqrt{2} \times \sqrt{2} \times 2$ 24-atoms rutile IrO_2 supercell was simulated for undoped IrO_2. For doping structures, one Ir atom in this $\sqrt{2} \times \sqrt{2} \times 2$ IrO_2 supercell was substituted by one Cu atom and one O atom was taken away for the Cu doping concentration of 12.5% (mole rate), while two Ir atoms in this supercell were replaced by two Cu atoms and two O atoms that were lost, which corresponded to a 25% Cu-substitution concentration. The Cu doping concentrations of both models were near the experimental input values of 10% and 30%, respectively. The (001) surfaces were chosen as slab models for pure IrO_2, $Ir_{0.9}Cu_{0.1}O_\delta$, and $Ir_{0.7}Cu_{0.3}O_\delta$, which were same as the common rutile (110) surfaces suggested by XRD results. These stoichiometric (001) surfaces with 3 × 1 supercell containing six O-Ir-O layers were optimized with the upper two tri-layers relaxed. Electronic density of states (DOS) was calculated using the tetrahedron method with Blöchl corrections for pure and Cu-doped IrO_2 systems.

Table.S1. The BET data of different composition of copper-iridium oxides

Catalysts	**$Cu_{0.1}Ir_{0.9}O_{\delta}$**	**$Cu_{0.3}Ir_{0.7}O_{\delta}$**	**$Cu_{0.5}Ir_{0.5}O_{\delta}$**	**$Cu_{0.7}Ir_{0.3}O_{\delta}$**	**$Cu_{0.8}Ir_{0.2}O_{\delta}$**	**$Cu_{0.9}Ir_{0.1}O_{\delta}$**	**IrO_2**
BET (m^2/g)	25.76	22.75	28.16	24.89	23.95	20.48	30.19

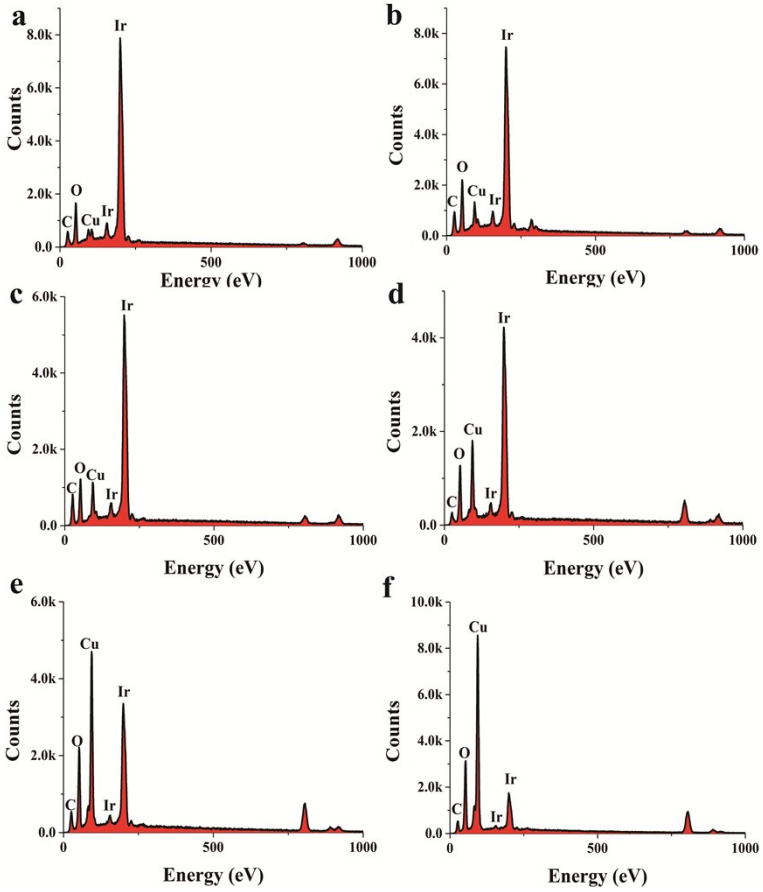

Fig. S1. EDS spectra for $Cu_xIr_{1-x}O_{\delta}$ compositions (a) for x=0.1, (b) for x=0.3, (c) for x=0.5, (d) for x=0.7, (e) for x=0.8, and (g) for x=0.9. The intensity from Ir gradually decreased as the amount of Cu doped increased.

Table. S2. Atomic percent of all elements in CuxIr1-xOδ compositions (x=0.1-0.9).

Catalysts	C (atom%)	O (atom%)	Ir (atom%)	Cu (atom%)	Ir/Cu[a]
$Cu_{0.1}Ir_{0.9}O_{\delta}$	14.76	52.41	29.54	3.27	9.03
$Cu_{0.3}Ir_{0.7}O_{\delta}$	18.86	58.41	15.69	7.03	2.23
$Cu_{0.5}Ir_{0.5}O_{\delta}$	26.48	44.82	14.85	13.85	1.07
$Cu_{0.7}Ir_{0.3}O_{\delta}$	12.4	39.78	14.39	33.42	0.43
$Cu_{0.8}Ir_{0.2}O_{\delta}$	23.46	40.57	7.03	28.94	0.242
$Cu_{0.9}Ir_{0.1}O_{\delta}$	20.36	41.78	2.95	34.91	0.085

[a]: The ratio of Ir/Cu (atom%) is a critical parameter for ensuring whether the composition coincides with the stoichiometric amounts. The value of Ir/Cu is shown to be close to the prepared stoichiometric compositions.

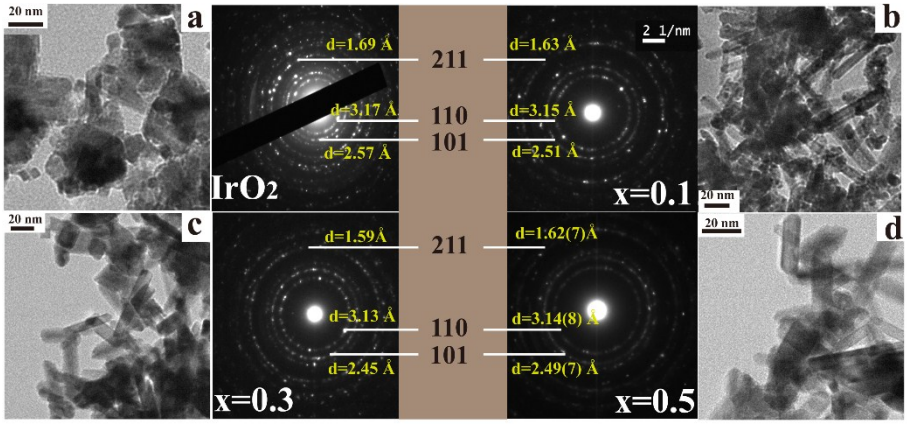

Fig.S2. TEM and SAED images of the $Cu_xIr_{1-x}O_{\delta}$ compositions.

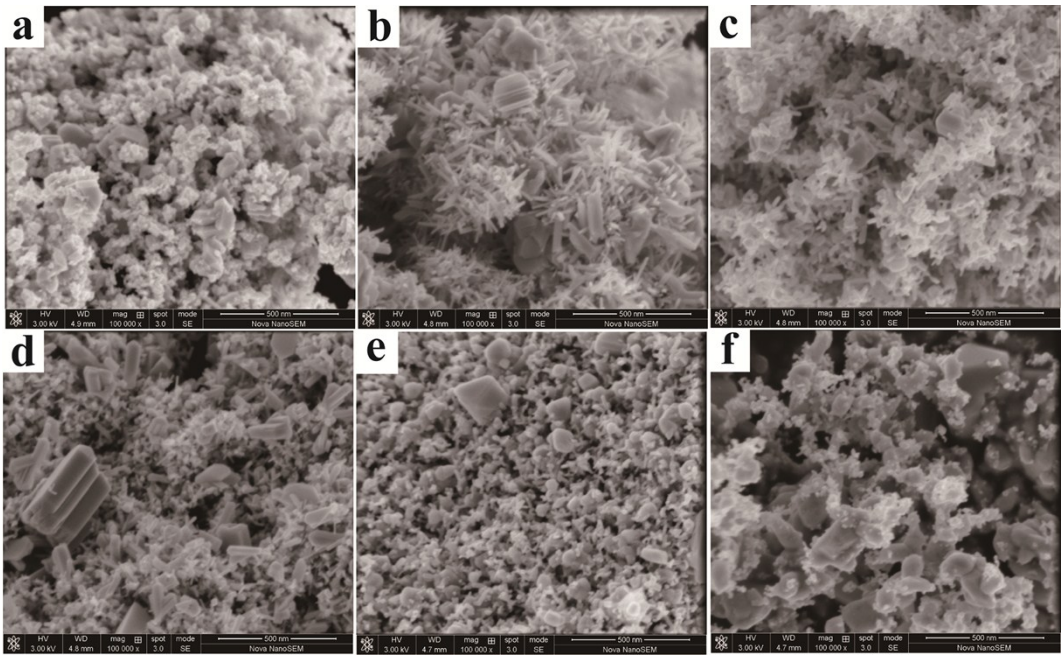

Fig.S3. SEM images of the $Cu_xIr_{1-x}O_\delta$ compositions, (a) for x=0.1, (b) for x=0.3, (c) for x=0.5, (d) for x=0.7, (e) for x=0.8, and (g) for x=0.9. Scale = 500 nm. A short rod-like morphology was clearly observed at x=0.3 and x=0.5, which indicated that the Cu doped into IrO_2 crystal made the crystalline grain have a preferred orientation.

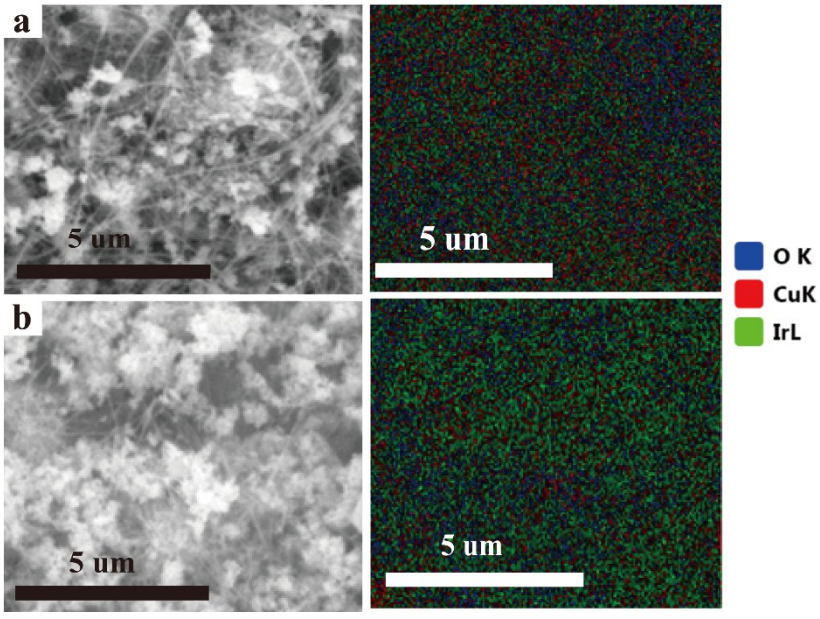

Fig.S4. EDX mapping of the $Cu_xIr_{1-x}O_\delta$ compositions, (a) with x=0.1 and (b) with x=0.3.

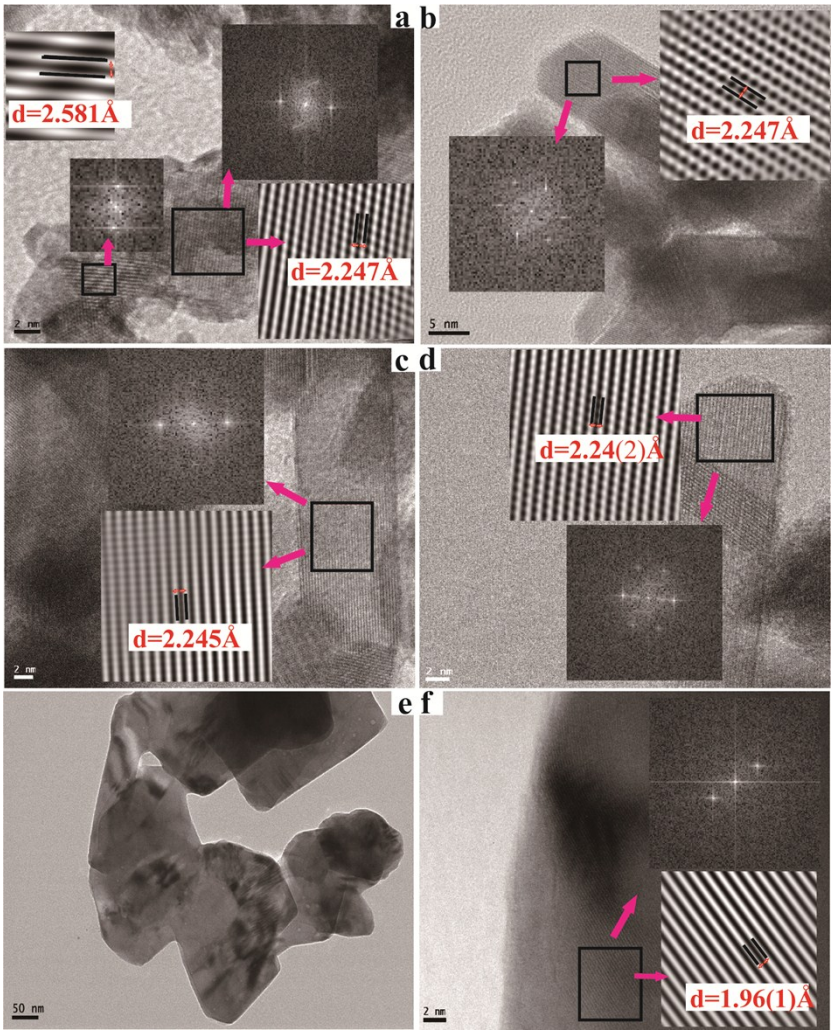

Fig. S5. High-resolution TEM (HRTEM) images of the prepared materials for (a) IrO_2, (b) $Cu_{0.1}Ir_{0.9}O_{\delta}$, (c) for $Cu_{0.3}Ir_{0.7}O_{\delta}$, (d) for $Cu_{0.5}Ir_{0.5}O_{\delta}$, (f) for CuO. (e) shows the TEM image of CuO. The insets show the fast Fourier transforms (FFTs) of the selected regions in the HRTEM, and the lattice fringe images correspond to the fast Fourier inversed transforms (IFFTs) in the selected regions. The FFTs indicate that the IrO_2 and Cu doped samples maintained a polycrystalline structure; however, CuO was found to be a monocrystal. The performed IFFTs were used to obtain clear lattice fringe images. The d-spaces in (b), (c) and (d) corresponding to the (200) plane were close to the value in (a).

Table.S3. Calculated lattice constants from peak locations and miller indices $Cu_xIr_{1-x}O_\delta$ compositions.

Catalysts	a=b-axis (Å)	c-axis (Å)	c/a ratio
IrO_2	4.498	3.154	0.7012[a]
$Cu_{0.1}Ir_{0.9}O_\delta$	4.4952	3.1488	0.7004(8)[a]
$Cu_{0.3}Ir_{0.7}O_\delta$	4.4912	3.146	0.7004(8)[a]
$Cu_{0.5}Ir_{0.5}O_\delta$	4.4907	3.1452	0.7003(8)[a]
$Cu_{0.7}Ir_{0.3}O_\delta$	4.4981	3.152	0.7007(4)[a]
$Cu_{0.8}Ir_{0.2}O_\delta$	4.4896	3.1455	0.7006(2)[a]
$Cu_{0.9}Ir_{0.1}O_\delta$	4.4915	3.1465	0.7005(4)[a]
$Cu_{0.1}Ir_{0.9}O_\delta$	4.5300	3.1723	0.7002(9)[b]
$Cu_{0.3}Ir_{0.7}O_\delta$	4.5218	3.1211	0.6902(3)[b]

[a] Calculated lattice constants from peak locations and miller indices.

[b] Based on DFT calculation.

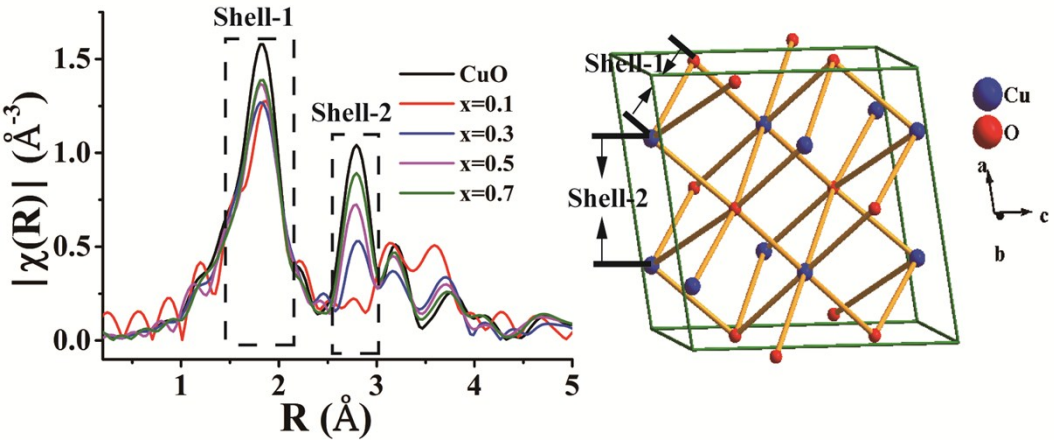

Fig.S6. (left) Fourier transforms of the k^3-normalized Cu-K edge EXAFS for $Cu_xIr_{1-x}O_\delta$ compositions. Phase correction was applied, and the k-range was 3-16 Å. (right) The sketch of one unit cell of CuO. The shell-1 formed due to a Cu-O bond (1.948 Å), and shell-2 corresponded to a Cu-Cu bond (2.898 Å); both are shown in the right sketch. It was noted that x=0.1 showed no Cu-Cu bond intensity, which indicated that Cu had totally penetrated the IrO_2 lattice and dispersed. Another interesting feature was that the Cu-Cu intensity gradually increased with an increasing amount of Cu amount, and the peak position of x=0.3 was larger than those of the other doped samples.

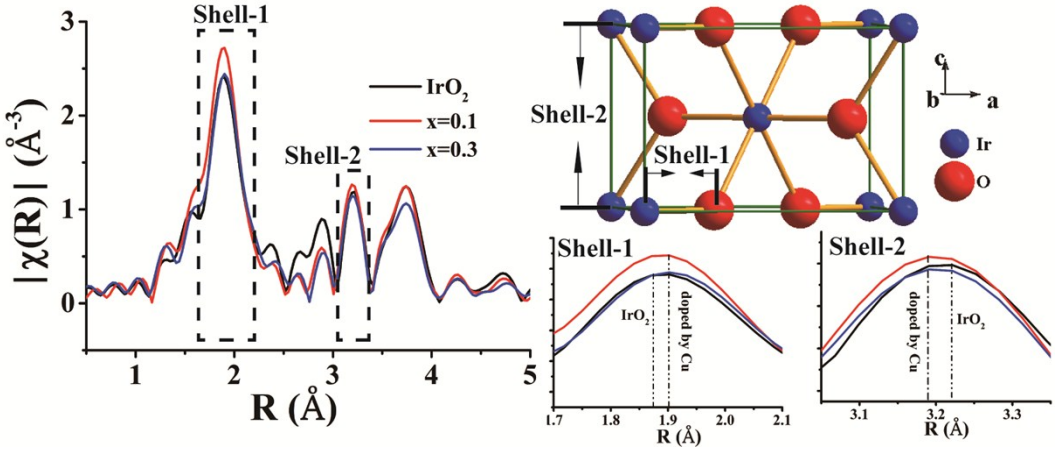

Fig.S7. (left) Fourier transforms of the k^3-normalized Ir-L_{III} edge EXAFS for $Cu_xIr_{1-x}O_\delta$ compositions. Phase correction was applied, and the k-range was 3-16 Å. (right) The sketch of one unit cell of IrO_2. The shell-1 formed due to an Ir-O bond (1.985 Å for the six Ir-O bonds in the IrO_6 coordination), and shell-2 formed due to an Ir-Ir bond (3.158 Å), which corresponds to the *c*-axis length; both are shown in the right sketch. It was found that the Ir-O bond marginally increased due to Cu doping; as mentioned in the text, the Ir-O bond might be transformed into 4S+2L from 4L+2S, and from ESAFS, we may infer that the incremental length of the apical Ir-O bond was larger than the reduced length of the planar Ir-O. From shell-2, the Ir-Ir bond was shown to decreased with doped Cu, which indicated a reduced *c*-axis length.

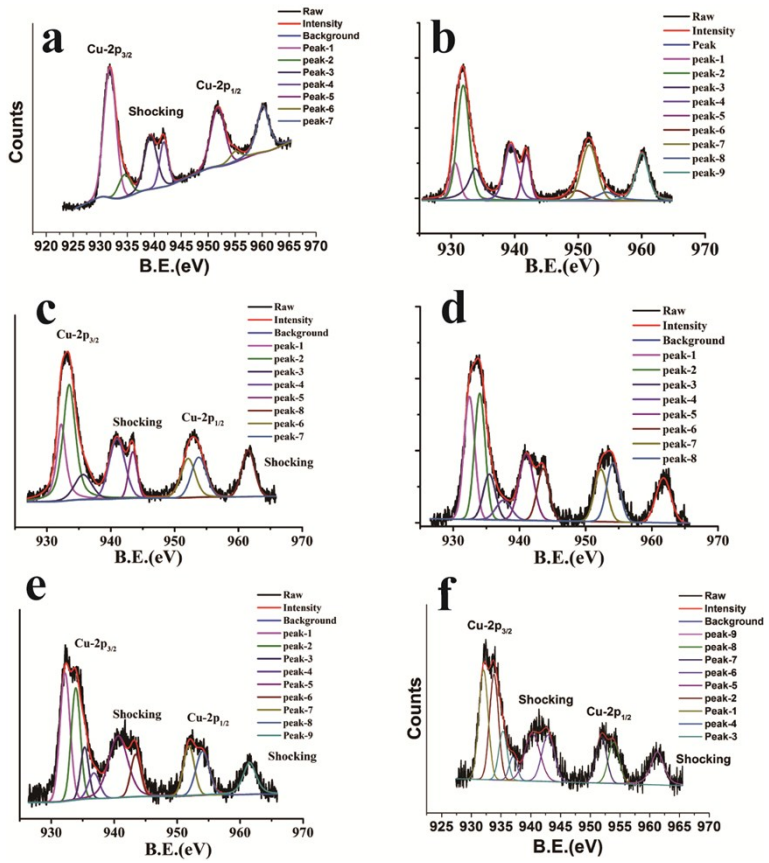

Fig.S8. High-resolution XPS spectra of Cu-2p for $Cu_xIr_{1-x}O_\delta$ compositions (a) for x=1, (b) for x=0.9, (c) for x=0.7, (d) for x=0.5, (e) for x=0.3, (f) for x=0.1. There were two types of Cu states in the samples without CuO, and the low valence state decreased with an increased amount of Cu doped. The shocking peak were observed in all samples, indicating that no Cu_2O existed in the samples even with a low amount of dopant (x=0.1).

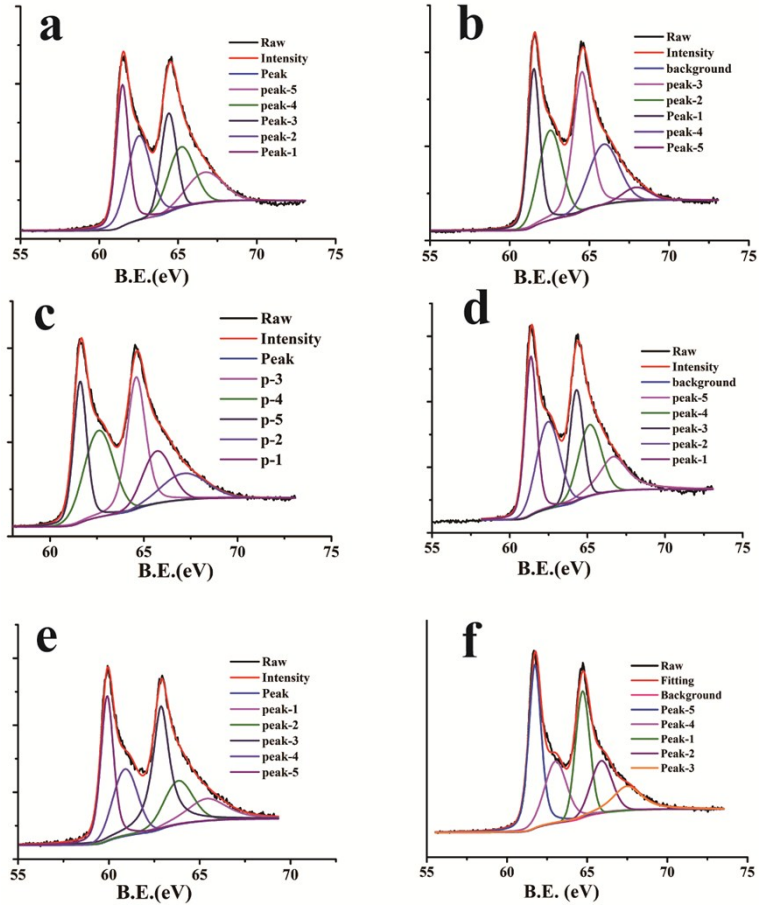

Fig.S9. High-resolution XPS spectra of Ir-4f for $Cu_xIr_{1-x}O_\delta$ compositions (a) for x=0.9, (b) for x=0.7, (c) for x=0.5, (d) for x=0.3, (e) for x=0.1, (f) for x=IrO_2. The fitting spectra showed a significant shoulder peak due to strong asymmetry peak type, and can be explanted by final-state effects[6, 7]; two possible final states are tenable to this asymmetry peak type: the low binding energy peak due to core hole is screened, while the high binding energy peak arising from the core hole is unscreened[8, 9]. The second model[10] treats the high core line as an unusually strong plasmon satellite relative to the low binding energy main peak, and broadened by conduction electron scattering, thus the high binding energy is so broadened. Therefore, we did not attribute the shoulder peak to the higher valence Ir.

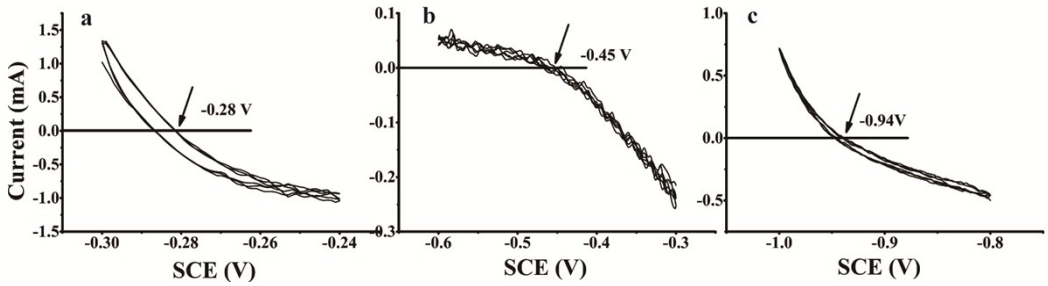

Fig.S10. CVs for RHE Calibration in the (a) acid solution 0.1 M $HClO_4$ ~pH=1, (b) neutral solution 0.2 M phosphate ~pH=7, and (c) basic solution 0.1 M KOH ~pH=13.RHE=SCE+0.28 V for the acid solution; the RHE=SCE+0.45 V for the neutral solution; and RHE=SCE+0.94 V for the basic solution.

a

$$M + H_2O \xrightarrow{\Delta G1} M - OH + H^+ + e$$
$$M - OH \xrightarrow{\Delta G2} M - O + H^+ + e$$
$$M - O + H_2O \xrightarrow{\Delta G3} M - OOH + H^+ + e$$
$$M - OOH \xrightarrow{\Delta G4} M + O_2 + H^+ + e$$

b

$$M + OH^- \xrightarrow{\Delta G1} M - OH + e$$
$$M - OH + OH^- \xrightarrow{\Delta G2} M - O + H_2O + e$$
$$M - O + OH^- \xrightarrow{\Delta G3} M - OOH + e$$
$$M - OOH + OH^- \xrightarrow{\Delta G4} M + O_2 + H_2O + e$$

Fig.S11. Proposed OER mechanism of metal oxides (a) in the acidic and neutral solutions (reactant was water), and (b) in the basic solution (reactant was hydroxide). For most metal oxides, step three included the formation of the oxy-hydroxide and was considered to be the RDS. As discussed in the text, the theoretical overpotential was defined as $\eta_{the}=\Delta G_3-1.229$ (V).

Table.S4. OER activity for the prepared catalysts in three types of pH solution.

Catalysts	**Acid**			**Neutral**			**Basic**		
	η (mV) @ *j*=10 mA/cm²	**Mass activity @ η=0.35 V (A/g)**	**Tafel slope (mV/dec)**	**η (mV) @ *j*=10 mA/cm²**	**Mass activity @ η=0.50 V (A/g)**	**Tafel slope (mV/dec)**	**η（mV）@ *j*=10 mA/cm²**	**Mass activity @ η=0.40 V (A/g)**	**Tafel slope (mV/dec)**
IrO_2	389	10	72	740	12	280	510	12.8	166
$Cu_{0.1}Ir_{0.9}O_\delta$	375	31.5	75	670	21.8	233	\	26.8	117
$Cu_{0.3}Ir_{0.7}O_\delta$	351	50	63	623	25.1	203	415	40	105
$Cu_{0.5}Ir_{0.5}O_\delta$	368	40	65	700	15.8	240	\	26.2	150
$Cu_{0.7}Ir_{0.3}O_\delta$	391	22	79	\	10	257	\	31	187
$Cu_{0.8}Ir_{0.2}O_\delta$	\	16.5	75	\	6.75	247	\	20	166
$Cu_{0.9}Ir_{0.1}O_\delta$	\	15	77	\	4.2	282	\	17.7	190

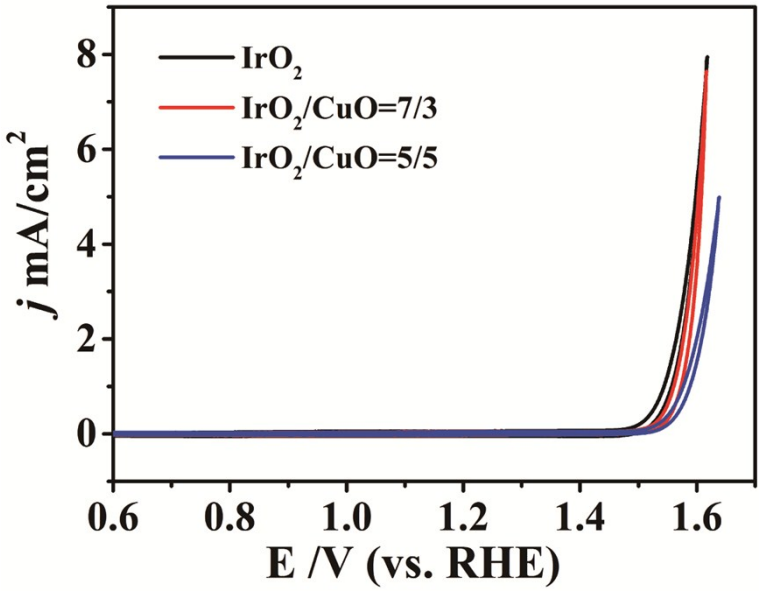

Fig.S12. Polarization curves for the OER of the mechanical mixing of CuO and IrO_2 materials in the acidic solution (0.1 M $HClO_4$). The mixtures of 7/3 and 5/5 were prepared by mixing 0.8 mg CuO with 5.2 mg IrO_2 and 1.6 mg CuO with 4.4 mg IrO_2, respectively, in accordance with the molar ratio of Ir/Cu in $Cu_{0.3}Ir_{0.7}O_\delta$ and $Cu_{0.5}Ir_{0.5}O_\delta$. The scan rate used was 10 mV/s.

Reference:

1. Y. Liang, Y. Li, H. Wang, J. Zhou, J. Wang, T. Regier and H. Dai, *Nat. Mater.*, 2011, **10**, 780-786.
2. G. Kresse and J. Furthmüller, *Phys. Rev. B*, 1996, **54**, 11169-11186.
3. G. Kresse and J. Hafner, *Phys. Rev. B*, 1993, **47**, 558-561.
4. J. P. Perdew and Y. Wang, *Phys. Rev. B*, 1992, **45**, 13244-13249.
5. J. P. Perdew, K. Burke and M. Ernzerhof, *Phys. Rev. Lett.*, 1996, **77**, 3865-3868.
6. A. Subedi, *Phys. Rev. B*, 2012, **85**, 020408.
7. J. Riga, C. Tenret-Noël, J. J. Pireaux, R. Caudano, J. J. Verbist and Y. Gobillon, *Phys. Scr.*, 1977, **16**, 351.
8. C. Körber, V. Krishnakumar, A. Klein, G. Panaccione, P. Torelli, A. Walsh, J. L. F. Da Silva, S. H. Wei, R. G. Egdell and D. J. Payne, *Phys. Rev. B*, 2010, **81**, 165207.
9. D. J. Payne, R. G. Egdell, W. Hao, J. S. Foord, A. Walsh and G. W. Watson, *Chem. Phys. Lett.*, 2005, **411**, 181-185.
10. A. Kotani, *J. Electron. Spectrosc. Relat. Phenom.*, 1996, **78**, 7-12.